Effect of turbulent flow on an atmospheric-pressure AC powered gliding arc discharge

Kong, Chengdong; Gao, Jinlong; Zhu, Jiajian; Ehn, Andreas; Aldén, Marcus; Li, Zhongshan

Published in:
Journal of Applied Physics

DOI:
10.1063/1.5026703

2018

Document Version:
Publisher's PDF, also known as Version of record

Journal of Applied Physics

Effect of turbulent flow on an atmospheric-pressure AC powered gliding arc discharge

Cite as: J. Appl. Phys. **123**, 223302 (2018); https://doi.org/10.1063/1.5026703
Submitted: 22 February 2018 • Accepted: 23 May 2018 • Published Online: 12 June 2018

Chengdong Kong, Jinlong Gao, Jiajian Zhu, et al.

Effect of turbulent flow on an atmospheric-pressure AC powered gliding arc discharge

Chengdong Kong,[1] Jinlong Gao,[1] Jiajian Zhu,[1,2] Andreas Ehn,[1] Marcus Aldén,[1] and Zhongshan Li[1]
[1]*Division of Combustion Physics, Lund University, P.O. Box 118, S-221 00 Lund, Sweden*
[2]*Science and Technology on Scramjet Laboratory, National University of Defense Technology, Changsha 410073, China*

(Received 22 February 2018; accepted 23 May 2018; published online 12 June 2018)

A high-power gliding arc (GA) discharge was generated in a turbulent air flow driven by a 35 kHz alternating current electric power supply. The effects of the flow rate on the characteristics of the GA discharge were investigated using combined optical and electrical diagnostics. Phenomenologically, the GA discharge exhibits two types of discharge, i.e., glow type and spark type, depending on the flow rates and input powers. The glow-type discharge, which has peak currents of hundreds of milliamperes, is sustained at low flow rates. The spark-type discharge, which is characterized by a sharp current spike of several amperes with duration of less than 1 μs, occurs more frequently as the flow rate increases. Higher input power can suppress spark-type discharges in moderate turbulence, but this effect becomes weak under high turbulent conditions. Physically, the transition between glow- and spark-type is initiated by the short cutting events and the local re-ignition events. Short cutting events occur owing to the twisting, wrinkling, and stretching of the plasma columns that are governed by the relatively large vortexes in the flow. Local re-ignition events, which are defined as re-ignition along plasma columns, are detected in strong turbulence due to increment of the impedance of the plasma column and consequently the internal electric field strength. It is suggested that the vortexes with length scales smaller than the size of the plasma can penetrate into the plasma column and promote mixing with surroundings to accelerate the energy dissipation. Therefore, the turbulent flow influences the GA discharges by ruling the short cutting events with relatively large vortexes and the local re-ignition events with small vortexes. *Published by AIP Publishing.* https://doi.org/10.1063/1.5026703

I. INTRODUCTION

Non-thermal plasma generated by atmospheric-pressure discharge has great potentials in various applications such as health care, material treatment, pollution controlling, combustion enhancement, transportation, and manufacturing.[1–7] However, the generation and maintenance of non-thermal plasmas in large power at atmospheric pressure is difficult because they easily transit to thermal plasmas due to thermal instability or thermionic emission of electrons from the cathode spot.[8] Several techniques can be considered to suppress the transition, such as covering the electrodes with insulator (e.g., DBD), using the nanosecond repetitively pulsed discharge,[9,10] or ballasting the discharge with a current-limiting resistor.[11] Recently, the gliding arc (GA) discharge sustained by an alternating current (AC) power supply was proposed as a simple and low-cost scheme to generate high-power non-thermal plasma at atmospheric pressure.[12–16]

In the GA discharge, the weakly ionized plasma column moves together with the surrounding gases, so the flow field and the plasma are strongly coupled to interact mutually. On the one hand, the flow field can be influenced by the moving plasma through gas heating and arc displacement.[17] On the other hand, the physical properties of the plasma column change under different flow rates. With the increase in the flow rate, the input power per unit discharge length, the electric field strength along the plasma column, and the impedance of arc column become larger.[18–21] The attainable maximum discharge length increased 30% with the flow rate varying from 5.4 m/s to 1.6 m/s under certain conditions.[19] Furthermore, at a high flow rate, the GA discharge becomes unstable, with wider fluctuations of discharge voltage[22] and breakdown voltage.[23] The transition of discharge modes was exhibited under different flow rates using a pin-to-pin electrode geometry and a nanosecond pulsed power supply.[9] The AC gliding arc discharge also demonstrated the transition between the diffusive glow type and the spark type[12,15] with the sparks appearing more frequently in a turbulent flow. In principle, the effect of the flow rate can be qualitatively explained using an energy balance. The high flow rate or strong turbulence accelerates the dissipation of active radicals or heat energy out of the plasma column and does thus change the discharge properties.[20]

In a turbulent flow, the gliding arc discharge behaves quite intricate. The high-speed diagnostic techniques, which can reveal the transient morphologies of discharges, are very useful for gaining a better understanding of the gliding arc behaviors in a turbulent flow. With the progress of simultaneously high-speed photography and electrical measurements, the spatiotemporally resolved characteristics of different GA discharges have been reported.[18,19,21] Richard *et al.*[18] studied the characteristics of DC GA discharge in air. Mitsugi *et al.*[21] investigated the gas flow dependence on

time-resolved dynamic behavior of AC argon gliding arc discharge. Zhang *et al.*[24] studied the electrical characteristics and dynamic behaviors of DC rotating GA discharge in nitrogen. In our recent work, the distinctive features of AC GA discharge in a turbulent air flow have been demonstrated, including the glow-type and spark-type discharges and their transition, the short-cutting events between electrodes and channel segments, and the afterglow plasma columns.[15] The previous investigations confirmed the complex interactions between the turbulent flow and the highly dynamic AC discharge. Nevertheless, the fundamental governing mechanisms behind these complex interactions are not clear, and thus a more comprehensive investigation is still needed.

This article aims at exploring the effect of turbulence on GA discharges explicitly by distinguishing the glow-type and spark-type discharges and clarifying their transition mechanisms. First, the glow-type and spark-type discharges are confirmed and defined. Then, the effects of the flow rate and the input power on the glow-spark transitions are exhibited. Transition mechanisms are finally investigated through the analysis of the transient discharge processes and the turbulence length scales.

II. EXPERIMENTAL SETUP

The details of the gliding arc discharge system have been described in the previous works.[3,12–15] Here, only a brief description is given. A schematic of the experimental setup is shown in Fig. 1. The system is operated in open air at atmospheric pressure. Two diverging hollow stainless steel tubes with an outer diameter of 3 mm and internally water-cooled are used as electrodes. One of the electrodes is connected to a 35 kHz alternating current (AC) power supply (Generator 9030 E, SOFTAL Electronic GmbH), whereas the other electrode is grounded. The rated output electric power of this power supply can be manually adjusted with a minimal step of 50 W from 400 W to 1400 W. The current and voltage values are automatically regulated by the power supply to control the output power. The discharge is ignited at the narrowest gap between the electrodes. The minimal gap distance is about 5 mm. The air flow controlled by a mass flowmeter from Bronkhorst is ejected through a 3-mm diameter hole between the two electrodes to push the generated plasma column upward.

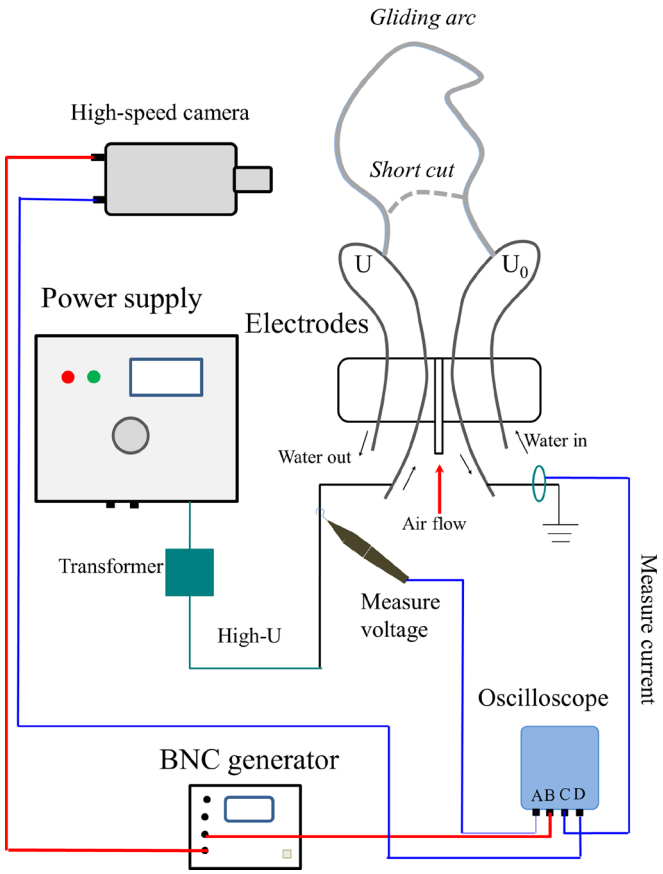

FIG. 1. Schematic of the experimental setup.

The current and the voltage are simultaneously measured using a current monitor (model 6585, Pearson Electronics) and a voltage probe (Tektronix P6015A). A high speed camera (HSC, Fastcam SA-X2, Photron) equipped with an objective lens (Micro-Nikkor 105 mm, f/2.8) is synchronized to capture the dynamics of the gliding arc discharge. The measurements were performed at a frame rate of 50 kHz with an exposure time of 16.25 μs. A pulse generator (BNC 575) is employed to synchronize the current/voltage and the HSC. The current and voltage signals together with the HSC gate signal and the external trigger signal are simultaneously recorded by a four-channel oscilloscope (PicoScope 4424, PS) at a sampling rate of 2 GHz.

III. RESULTS AND DISCUSSION

A. Types of the gliding arc discharge

Figure 2 illustrates the current waveforms sampled during the initial breakdown and the shortcutting events, together with snapshots captured by the high speed camera. The gliding arc discharge is initiated with a breakdown at the shortest gap between the diverging electrodes. The breakdown process is accompanied by intensive light emission and a large electric current [see Fig. 2(a)]. After this formation process, the arc moves and elongates with the gas flow while undergoing the transitions between different discharge types. In the experiment, two discharge types were discriminated according to the apparent emission intensity and the current amplitude. At 69.34 ms and 91.22 ms, the discharge columns have relatively weak and diffusive emissions [see Figs. 2(c) and 2(e)], corresponding to the so-called glow-type discharge, with a current of the order of hundreds milliamperes. However, during short cutting events at 69.42 ms and 91.31 ms, which are a sudden bridge of the stretched plasma column[15] [see Figs. 2(d) and 2(f)], the emission from the GA channel becomes much brighter, along with a current spike of several amperes. It corresponds to a spark-type discharge. During the initial breakdown at the shortest electrode gap, the discharge is spark-type, and typically it will transit to a glow-type discharge after several repetitive sparks [see Fig. 2(b)].

To analyze the glow-type and the spark-type discharge, a distribution function of the peak value of the current per AC power period is derived under different flow rates and

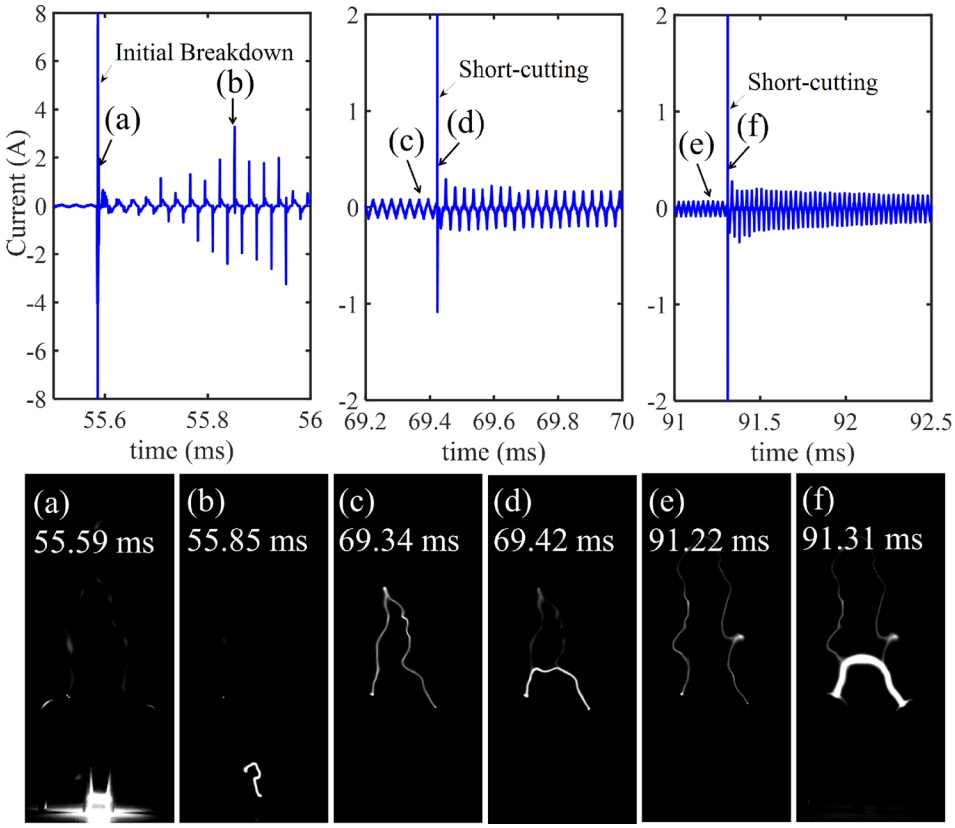

FIG. 2. Current waveforms sampled during the initial breakdown and the short cutting events, together with snapshots (a)–(f) captured by the high speed camera. The high-speed images are acquired with an exposure time of 16.25 μs.

input electric powers, as exhibited in Fig. 3. The electric powers are calculated from the measured current and voltage, different from the preset power of the power supply. The y-axis represents the counted number of peak current per period within a time span of 1 s. For a low flow rate, the peak current per period is mostly smaller than 1 A, corresponding to the glow type. Nevertheless, the large current spikes from sparks become more frequent as the flow rate is larger. In order to quantitatively distinguish the glow and the spark types from the electrical parameters, a transition peak current is defined as 1 A here. Below 1 A, the discharge belongs to the glow type. Otherwise, it belongs to the spark type. It should be noted that the duration of spark-type discharge is less than 1 μs. It means the spark-type discharge is

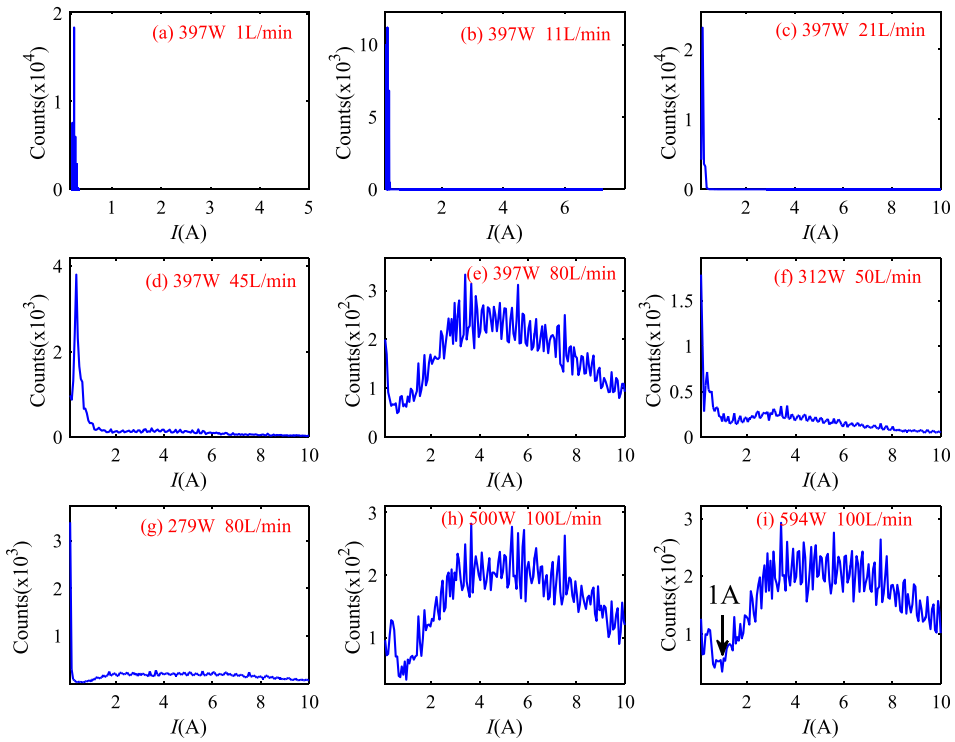

FIG. 3. Current distributions under different flow rates and electric powers.

a pulsed phenomenon while the glow-type discharge is more common and continuous.

B. Effects of input electric power and flow rate on the discharge characteristics

The glow-spark transition is an important discharge feature because the discharge type can influence the plasma properties such as emission spectra and radical concentrations. Here, the dimensionless rate of sparks, which is defined as the ratio of the frequency of the current spikes (>1A) to the frequency of the AC power supply, is introduced to quantify the glow-spark transition rate in statistics, as demonstrated in Fig. 4. The acquired current signal is used to calculate the dimensionless rate of sparks. The results indicate that the rate of sparks rises up with respect to the flow rate along an S-shaped curve form. Three regimes are qualitatively defined according to this S-shaped curve. Regime 1, where the rate of sparks is defined to be below 0.01, represents a glow mode of discharge which has occasional short cuttings of the plasma column. Regime 3 represents the full spark mode of discharge where the current spikes emerge in almost every period. Regime 2 shows the transition from the glow mode to the full spark mode.

With the increase in the rated input electric power, Regime 2 in Fig. 4 shifts to the right side, meaning a larger flow rate for the glow-to-spark mode transitions. However, this power effect becomes negligible above 500 W so that the curves are nearly overlapped. For a high flow rate of around 60 l/min, the rate of sparks is almost independent of the input power. To clarify the effects of input power and the flow rate on the transition, a regime diagram of the glow mode and the spark mode with respect to the input power and the flow rate is drawn in Fig. 5. In Fig. 5, the discharge with the rate of sparks below 0.01 is regarded as a glow mode of discharge, otherwise as a spark mode. We can find that the critical flow rate for the glow-spark mode transition increases logarithmically with the input power. At high flow rates, the transition point becomes less sensitive to the input power.

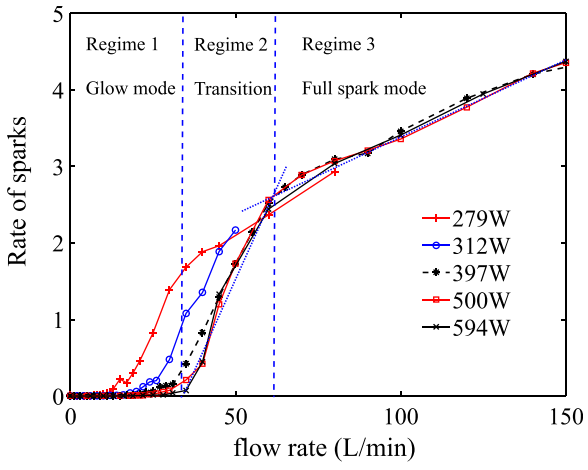

FIG. 4. Dimensionless rate of sparks with respect to flow rate under different input electric powers.

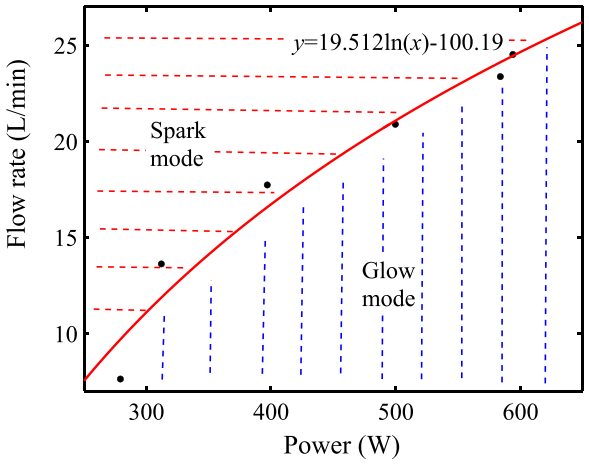

FIG. 5. A regime diagram of the glow/spark models with respect to the electric power and the flow rate.

The instantaneous length of the plasma column was derived from the high-speed images, as plotted in Fig. 6. The length was evaluated using two-dimensional images rather than the real three-dimensional structure of the plasma column, which may underestimate the length of plasma columns by up to 25%.[25] The inset of Fig. 6 indicates that at a fixed flow rate (e.g., 7 l/min), the length fluctuates typically with a sawtoothed curve owing to the short cutting events. Averagely, the length of the plasma column decreases as the flow rate is larger at a fixed input power. It is largely attributed to the frequent short cutting event to confine the growth of length of the plasma column at a higher flow rate.

C. Instantaneous glow-spark transition processes

Figure 7 illustrates the snapshots of the instantaneous glow-spark-glow transition process, together with associated current and voltage curves. For the considered time period in Fig. 7, the first spark occurs at 1.96 ms ~ 1.98 ms via a short cutting event. Subsequently in the following 1 ms, current spikes and the bright plasma column (i.e., sparks) appear repetitively. The repetition rate is mainly controlled by the voltage recovery rate, which is dependent on the characteristics of the

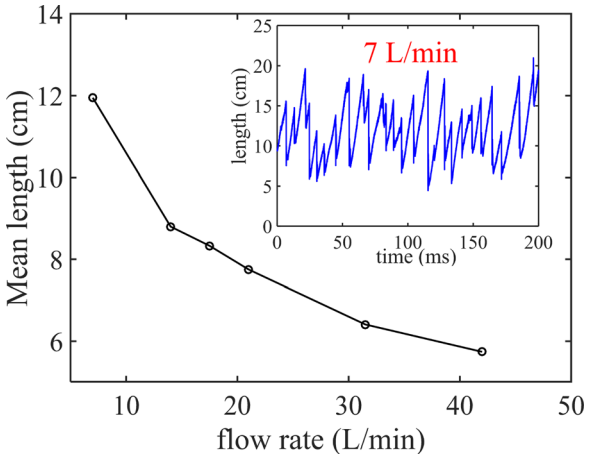

FIG. 6. Time-averaged length of the gliding arc with respect to the flow rate. Inset is the instantaneous length of the plasma column at a flow rate of 7 l/min.

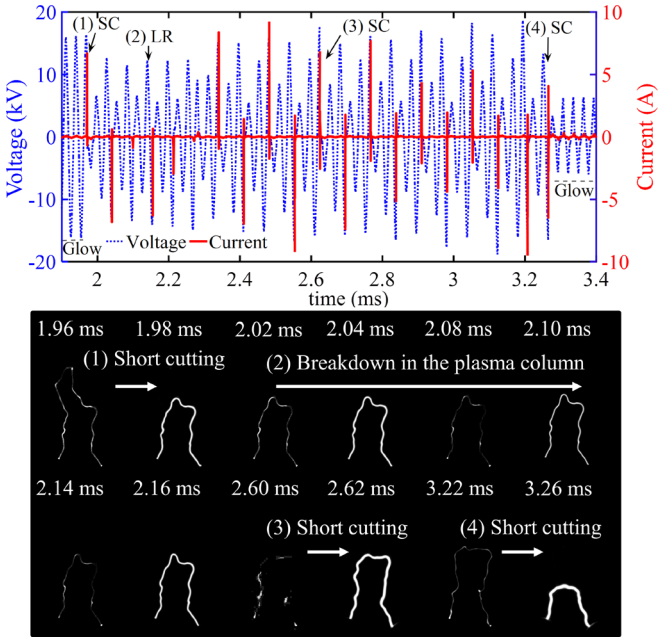

FIG. 7. Snapshots of glow-to-spark-to-glow transitions, combined with the current and voltage curves. The flow rate is 17.5 l/min. SC: short-cutting, LR: local re-ignition.

power supply.[15] Different from the short-cutting events, these current spikes are attributed to the breakdown along the glow-type plasma column when the electric field strength (E) is above a threshold. It is here called as "local re-ignition." A small short cutting event is detected at 2.60 ms ~ 2.62 ms, but it does not disturb the repetitive local re-ignition events. However, at 3.22 ms ~ 3.26 ms, another short cutting event occurs which changes the morphology of the plasma column and consequently stops the repetitive local re-ignition process. Then, the gliding arc returns to the glow type. This recorded glow-spark transition manifests that the short cutting events control the glow-to-spark and spark-to-glow transitions and the sparks emerge owing to the short-cutting events or the local re-ignition events.

In order to gain more insights into the fast short-cutting process, the frame rate of the high-speed camera is increased to 200 kHz. Interestingly, two types of short-cutting processes were found as shown in Figs. 8 and 9. Figure 8 shows the snapshots of the glow discharges during the short cutting process, combined with the corresponding current-voltage (I-U) curves. The result reveals a relatively slow short cutting event for the illustrated case. Initially, some small ionized spot emerges around 1 cm away from the plasma column and then grows bigger until the plasma is totally short-cut. The current and voltage waveforms do not change until the plasma column is totally bridged. Afterwards the current peak increases without current spikes and the voltage drops from 6.4 kV to 3.9 kV. The total duration of this short-cutting event is as long as around 200 μs. This mild short-cutting event is here defined as a glow short cutting event to distinguish it from the spark short cutting event. Figure 9 shows snapshots of a discharge during a spark short cutting event, which is much faster compared to the glow short cutting event. As illustrated in Fig. 9, the plasma column is short-cut within 28 μs. Furthermore, two plasma columns are detected during breakdown. It takes nearly 0.3 ms for these two channels to fuse together.

D. Mechanisms of the short cutting and the local re-ignition events

Essentially, the short cutting and the local re-ignition events both belong to electrical breakdowns, which occur

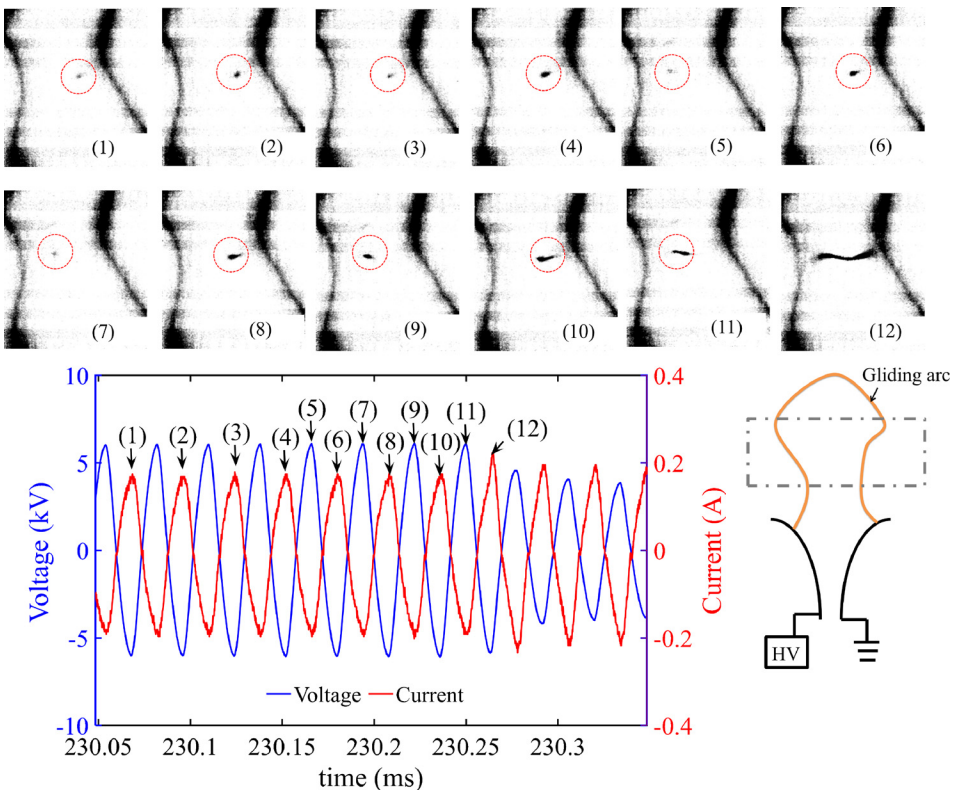

FIG. 8. Snapshots of discharge during a glow short cutting event, together with the corresponding current-voltage (I-U) curves. The dashed circle marks the locally ionized spot.

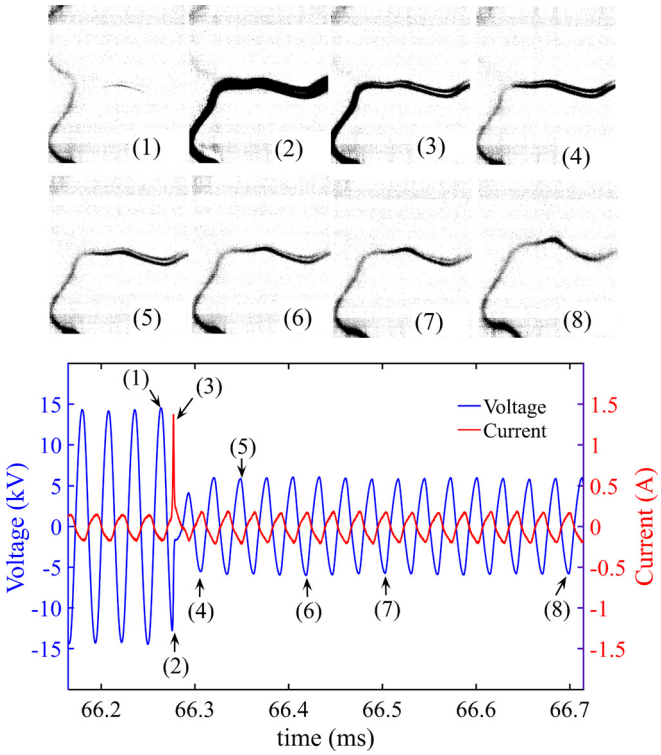

FIG. 9. Snapshots of discharge during a spark short cutting event, together with the corresponding current-voltage (I-U) curves.

when E field reaches a threshold. The air breakdown has been widely studied and its breakdown strength ($E_{bk,0}$) at room temperature and 1 atm is normally 3 MV/m. The uniqueness of short-cutting and local re-ignition events are the complex and non-uniform environments along the breakdown channels. During the short cutting event, a new conductive pathway is formed in a relatively cold place neighbouring the plasma column to bridge the upper part of the plasma column. By estimating the electric potential difference and distances between the ends of the new conductive pathway, the mean breakdown strength can be calculated to vary from 150 kV/m to 200 kV/m during the short cutting events. The local re-ignition event occurs in the glow-type plasma column, which contains active radicals and has a higher temperature than the surroundings. Its breakdown strength is estimated to be 120 kV/m.[15] These breakdown strengths of short-cutting and local re-ignition events are much smaller than that of pure air at room temperature, which can result from the thermal effect and the kinetic effect. Assuming a pure thermal effect on breakdown (i.e., $E_{bk}/N =$ constant, N is the molecular number density), an effective temperature (T_{eff}) can be defined from the following equation:

$$T_{eff} = T_0 \times E_{bk,0}/E_{bk}, \quad (1)$$

where T_0 and $E_{bk,0}$ are the temperature and the corresponding breakdown strength of non-ionized air, respectively; E_{bk} is the breakdown strength for the short cutting or local re-ignition event. T_{eff} for short-cutting events and local re-ignition events are estimated to be 4500–6000 and 7500 K, respectively, which are much higher than the measured translational temperature of the GA channel (~1100 K).[26] It implies that some non-thermal effects work to promote the breakdown. For instance, active species such as N_2*, OH*, and NO* have much higher vibrational and electronic temperatures that enhance ionizations.[26]

The short-cutting event initiates 1 cm away from the plasma core. According to the previous temperature mapping,[26] the local translational temperature is less than 1000 K. It is quite surprising that the effective temperature of short-cutting events can be above 4000 K. We infer that some active radicals survive a long time to drift centimeters away from the plasma channel. The relatively large variation of breakdown strengths for the short-cutting events results from the different breakdown types. As shown in Figs. 8 and 9, the glow short-cutting event occurs by slowly pre-ionizing the local spot. Its initial breakdown strength should be low (~150 kV/m). The spark short-cutting event occurs through fast streamer processes, and thus a large electric field strength (~200 kV/m) is needed for fast ionizations.

E. Impacts of heterogeneous turbulent flows on GA discharges

A turbulent flow usually undergoes complex transformations that are hard to foresee in detail, but qualitatively the turbulent flow can be decomposed into a laminar flow and eddying motions over a wide range of length scales from the integral length scales to the Kolmogorov length scales. Figure 10 shows a schematic flow field, which is composed of a laminar jet flow and vortexes with different sizes. The

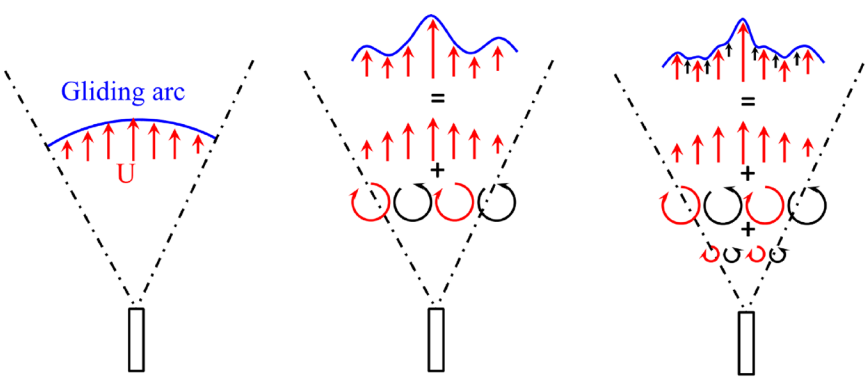

FIG. 10. Schematic morphology of the plasma column in different flow fields. The blue curve represents the gliding arc.

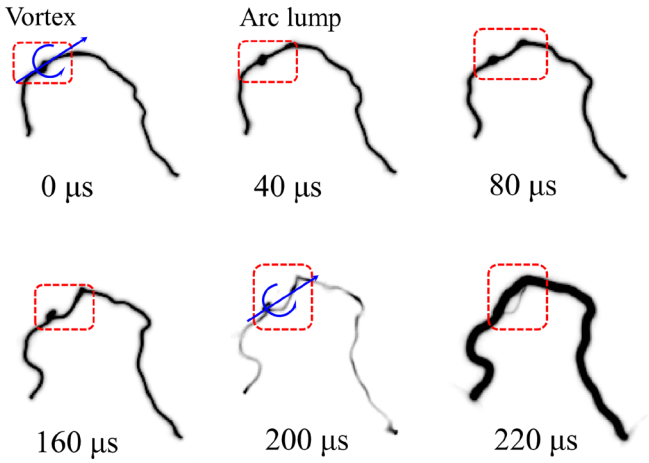

FIG. 11. A trajectory of the plasma column following a vortex tube. The jet flow rate is 42 l/min.

size of vortexes can be varied by adjusting the jet flow rate. Since the gliding arc is a weakly ionized gaseous mixture, it behaves like a flexible filament to follow the streamlines well. Hence, the morphology of the plasma column in a two-dimensional flow field can be schematically demonstrated in Fig. 10. In laminar flow, the gliding arc column is not wrinkled [see Fig. 10(a)]. When vortexes are added to represent the turbulent flow, the plasma column will be wrinkled and stretched [see Fig. 10(c)]. In a real flow, the turbulence is three-dimensional and the plasma column can be twisted as well. Figure 11 illustrates the dynamic interaction between the vortex tube and the plasma column. At first, a small vortex interacts with the arc column and twists it, forming a bright "lump" in Fig. 11. The arc column surrounding this "lump" will twist and elongate within the next 200 μs due to the expanding vortex tube, and finally becomes straight because of a short cutting event.

The E field, which controls the occurrence of short-cutting and local re-ignition events, depends not only on the voltage difference between the electrodes but also on the properties and morphology of the plasma column. The flow field impacts the E field from two aspects indirectly. First, the gliding arc can stretch, twist, and wrinkle to follow the streamlines flexibly and thus change the location and shape of the plasma column and consequently the E field. When the plasma channel segments are close to each other, the local E can reach the breakdown strength for short cutting events easily. Therefore, the arc movement on a relatively large length scale triggers the short cutting event. Second, the E in the plasma column increases with the flow rate. Figure 12 demonstrates the voltage amplitude with respect to the length of the plasma column under different flow rates. The slopes represent the averaged E ($\overline{E}$) in the plasma column. $\overline{E}$ increases together with the impedance of the plasma column as the flow rate grows. When the flow rate is as large as 42 l/min, the local re-ignition event occurs frequently since $\overline{E}$ is above the threshold for the local re-ignition event.

The increment of E in strong turbulence can be explained with the local energy balance. A local plasma channel segment can be treated as a cylinder with a radius of r_{arc} and a length of δl. Using the steady-state approximation, the energy balance around this local plasma column is expressed as

$$\delta P \approx 2\pi r_{arc}\delta l \times k_{\mathrm{eff}} \times \left.\frac{dT}{dr}\right|_{r=r_{arc}}, \tag{2}$$

where δP is the input power; k_{eff} is the effective thermal conductivity; $\left.\frac{dT}{dr}\right|_{r=r_{arc}}$ is the effective temperature gradient at r equal to r_{arc}. It should be clarified that for a non-thermal plasma the energy transport includes not only the heat conductivity but also the mass transport of active species such as O, OH, and NO. Here, the thermal conductivity formula with effective parameters is used to describe the energy transport qualitatively. The effective temperature gradient is linearly estimated as follows:

$$\left.\frac{dT}{dr}\right|_{r=r_{arc}} \approx (T_{\mathrm{arc}} - T_{\mathrm{sur}})/\delta_{\mathrm{arc}}, \tag{3}$$

where T_{arc} and T_{sur} are the effective temperatures of plasma column and surrounding gas, respectively; δ_{arc} represents a length scale to define the effective temperature gradient around the plasma column. In laminar flow, the energy transport is governed by the molecular diffusion in the plasma column, and thus δ_{arc} is of the same order as r_{arc}. In turbulent flow, the transport rate is dependent on the Kolmogorov scale. When the considered length scale is smaller than the Kolmogorov length scale (l_{K}), the transport is still governed by the molecular diffusion. Otherwise, convective mixing must be considered. Here, δ_{arc} can be estimated as

$$\delta_{\mathrm{arc}} \approx \min(r_{arc}, l_K). \tag{4}$$

It means that when r_{arc} is smaller than l_{K}, the turbulent effect on the energy dissipation is weak and thus the energy dissipation rate is similar to that in laminar flow. However, when l_{K} is smaller than r_{arc}, the energy dissipation is controlled by the turbulent mixing. The input power, δP, is derived from the current and the local voltage drop, written as

$$\delta P = I \times \delta U = I \times E_{\delta l} \times \delta l, \tag{5}$$

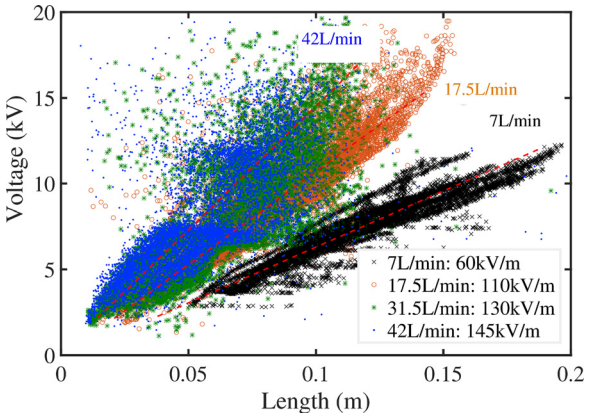

FIG. 12. Voltage amplitude of the AC power supply with respect to the length of the plasma column at different flow rates. The slopes, which represent the mean electric field ($\overline{E}$), are around 60 kV/m at 7 l/min, 110 kV/m at 17.5 l/min, 130 kV/m at 31.5 l/min, and 145 kV/m at 42 l/min.

where I is the current; δU is the local voltage drop; and $E_{\delta l}$ is the local electric field strength. Combining Eqs. (2)–(5) yields the local electric field strength, given by

$$E_{\delta l} \approx \frac{2\pi r_{\mathrm{arc}} k_{\mathrm{eff}} (T_{\mathrm{arc}} - T_{\mathrm{sur}})}{\min(r_{arc},\, l_K) I}. \tag{6}$$

Equation (6) indicates that if l_{K} is smaller than r_{arc}, E increases as the turbulent length scale decreases.

For a jet flow, the turbulence intensity and the distribution of l_{K} are heterogeneous in space.[27] Therefore, the local E along the plasma column should not be the same. This can be partially confirmed from the non-uniform emission of discharges in Fig. 7. In Sec. III D, the mean breakdown strength for the local re-ignition events has been estimated to be 120 kV/m. If the non-uniformity of E is considered, the peak value must be larger. Non-uniformity makes the situations much more complex, and direct measurement or simulation of E profile is of significance to study the discharge characteristics (e.g., short cutting and local re-ignition events) in the future.

Overall, there are two basic pathways for the turbulence to impact the gliding arc. On a relatively large length scale, the morphology of plasma column is altered to trigger the short cutting events, while on a length scale smaller than the arc radius, the energy dissipation around the plasma column is enhanced to trigger the local re-ignition. To summarize the impacts of turbulence on the gliding arc, a regime diagram is plotted to indicate different discharge forms in Fig. 13. The x-coordinate represents the ratio of the arc length (l_{arc}) to the shortest distance between the cathode and anode spots (l_{spot}), which describes the basic morphologies of the gliding arc column. The y-coordinate is the ratio of the arc radius to the Kolmogorov length scale (l_{K}). Three regimes are identified. The first regime [see Fig. 13(a)] includes a non-wrinkled plasma column, which was detected in laminar flow using electrodes with small gaps.[19,21] In this regime, the plasma column is short and difficult to wrinkle or stretch by the flow. With elongation, the gliding arc column becomes much easier to wrinkle, stretch, and twist, thus resulting in

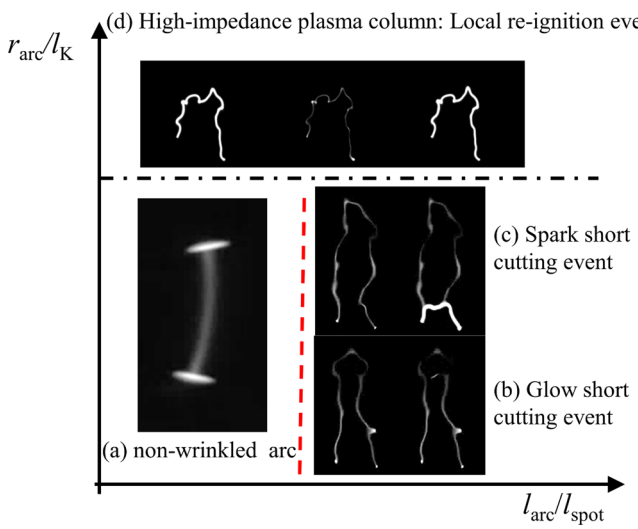

FIG. 13. A regime diagram of gliding arc in different flow fields.

frequent occurring of short cutting events. There are two types of short cutting events, including the glow short cutting event [see Fig. 13(b)] and the spark short cutting event with current spikes [see Fig. 13(c)]. The glow short cutting event occurs due to the locally long-lived ionized spot. This ionized spot could survive around 0.2 ms as illustrated in Fig. 8. However, in highly turbulent flow, the pre-ionized spots dissipate fast and thus the short cutting event tends to be of spark type. When the turbulence is so strong that the Kolmogorov length scale is much smaller than the arc radius, E inside the plasma column increases [see Eq. (6)] to trigger the local re-ignition events [see Fig. 13(d)]. This diagram can be used to explain the three regimes shown in Fig. 4. In the regime 1 of Fig. 4, the flow field is largely laminar and short cutting events occur mainly on the top parts of the plasma column to find a path with lower impedance and restrain the length of gliding arc. The turbulent dissipation is so weak that the short cutting events are mild without current spikes. With the flow rate increasing, the rate of sparks rises up from regime 1 to regime 2. This transition is mainly attributed to the short-cutting induced sparks. When the flow rate is very high, the electric field strength along the plasma column will be above the threshold of local re-ignition. Therefore, the transition from regime 2 to regime 3 is owing to the frequent local re-ignition events.

IV. CONCLUSIONS

The effect of turbulent jet flow on the characteristics of gliding arc discharge is analyzed based upon the simultaneous high-speed photography and electrical measurements. Two discharge types, glow type and spark type, are discriminated according to the peak current value. The occurrence rate of these two discharge types is controlled by the flow rate and the input power. The rate of sparks increases with the flow rate but decreases with the input power in a moderate turbulent flow. If the flow is highly turbulent, the effect of changing the input power becomes weak.

Physically, the spark-type discharge is controlled by the short cutting and local re-ignition events. At a relatively small flow rate, short cutting events dominate. When the turbulence is strong enough, the impedance of the plasma column and the electric field strength both rise up to induce the local re-ignition events. The turbulent flow can be regarded as a combination of laminar flow and vortexes with different length scales. Considering the specific filamentary morphology, the response of the gliding arc discharge channel to vortexes depends on the length scale. Relatively large vortexes can wrinkle, stretch, and twist the plasma column to trigger the short cutting event, while the vortexes with a length scale smaller than the radius of the plasma column enhances the energy dissipation to induce the local re-ignition event.

ACKNOWLEDGMENTS

This work was financially supported by the Swedish Energy Agency, the Swedish Research Council, the Knut and Alice Wallenberg Foundation, the European Research Council, and the National Natural Science Foundation of China (Grant No. 51606217).

[1]D. Rusterholtz, *Nanosecond Repetitively Pulsed Discharges in Atmospheric Pressure Air* (Ecole Centrale, Paris, 2012).
[2]T. Ombrello, X. Qin, Y. Ju, A. Gutsol, A. Fridman, and C. Carter, AIAA J. **44**, 142 (2006).
[3]Y. Kusano, B. F. Sorensen, T. L. Andersen, H. L. Toftegaard, F. Leipold, M. Salewski, Z. Sun, J. Zhu, Z. Li, and M. Alden, J. Phys. D: Appl. Phys. **46**, 135203 (2013).
[4]Y. Kusano, J. Adhes. **90**, 755 (2014).
[5]C. Du, J. Yan, X. Li, B. Cheron, X. You, Y. Chi, M. Ni, and K. Cen, Plasma Chem. Plasma Proces. **26**, 517 (2006).
[6]M. J. Gallagher, R. Geiger, A. Polevich, A. Rabinovich, A. Gutsol, and A. Fridman, Fuel **89**, 1187 (2010).
[7]V. Dalaine, J. M. Cormier, S. Pellerin, and P. Lefaucheux, Appl. Phys. **84**, 1215 (1998).
[8]L. Prevosto, H. Kelly, B. Mancinelli, J. C. Chamorro, and E. Cejas, Phys. Plasmas **22**, 023504 (2015).
[9]C. Zhang, T. Shao, P. Yan, and Y. Zhou, Plasma Sources Sci. Technol. **23**, 035004 (2014).
[10]D. Pai, D. Lacoste, and C. O. Laux, Plasma Sources Sci. Technol. **19**, 065015 (2010).
[11]M. Janda, Z. Machala, L. Dvonc, D. Lacoste, and C. O. Laux, J. Phys. D: Appl. Phys. **48**, 035201 (2015).
[12]J. Zhu, J. Gao, Z. Li, A. Ehn, and M. Alden, Appl. Phys. Lett. **105**, 234102 (2014).
[13]Z. Sun, J. Zhu, Z. Li, M. Alden, F. Leipold, M. Salewski, and Y. Kusano, Opt. Express **21**, 6028 (2013).
[14]J. Zhu, Z. Sun, Z. Li, A. Ehn, M. Alden, M. Salewski, F. Leipold, and Y. Kusano, J. Phys. D: Appl. Phys. **47**, 295203 (2014).
[15]J. Zhu, J. Gao, A. Ehn, M. Alden, Y. Kusano, and Z. Li, Phys. Plasmas **24**, 013514 (2017).
[16]A. Fridman, S. Nester, L. A. Kennedy, A. Saveliev, and O. Mutaf-Yardimci, Prog. Energy Combust. **25**, 211 (1999).
[17]N. Balcon, N. Benard, P. Braud, A. Mizuno, and E. Moreau, J. Phys. D: Appl. Phys. **41**, 205204 (2008).
[18]F. Richard, J. M. Cormier, S. Pellerin, and J. Chapelle, J. Appl. Phys. **79**, 2245 (1996).
[19]O. Mutaf-Yardimci, A. V. Saveliev, A. Fridman, and L. A. Kennedy, J. Appl. Phys. **87**, 1632 (2000).
[20]G. Xu and X. Ding, IEEE Trans. Plasma Sci. **40**, 3458 (2012).
[21]F. Mitsugi, T. Ohshima, H. Kawasaki, T. Kawasaki, S. Aoqui, T. Baba, and S. Kinouchi, IEEE Trans. Plasma Sci. **42**, 3681 (2014).
[22]Z. Wang, G. Chen, Z. Wang, N. Ge, H. Li, and C. Bao, J. Appl. Phys. **110**, 033308 (2011).
[23]C. Zhang, T. Shao, J. Xu, H. Ma, L. Duan, C. Ren, and P. Yan, IEEE Trans. Plasma Sci. **40**, 2843 (2012).
[24]H. Zhang, F. Zhu, X. Li, and C. Du, Plasma Sci. Technol. **19**, 045401 (2017).
[25]J. Zhu, J. Gao, A. Ehn, M. Alden, Z. Li, D. Moseev, Y. Kusano, M. Salewski, A. Alpers, P. Gritzmann, and M. Schwenk, Appl. Phys. Lett. **106**, 044101 (2015).
[26]J. Zhu, A. Ehn, J. Gao, C. Kong, M. Alden, M. Salewski, F. Leipold, Y. Kusano, and Z. Li, Opt. Express **25**, 20243 (2017).
[27]S. P. Pope, *Turbulent Flows* (Cambridge University Press, 2000).